

RESEARCH ARTICLE SUMMARY

CLIMATE IMPACTS

Temperature-dependent hypoxia explains biogeography and severity of end-Permian marine mass extinction

Justin L. Penn*, Curtis Deutsch*, Jonathan L. Payne, Erik A. Sperling

INTRODUCTION: Climate change triggered by volcanic greenhouse gases is hypothesized to have caused the largest mass extinction in Earth's history at the end of the Permian Period (~252 million years ago). Geochemical evidence provides strong support for rapid global warming and accompanying ocean oxygen (O₂) loss, but a quantitative link among climate, species' traits, and extinction is lacking. To test whether warming and O₂ loss can mechanistically account for the marine mass extinction, we combined climate model simulations with an established ecophysiological framework to predict the biogeographic patterns and severity of extinction. Those predictions were confirmed by a spatially explicit analysis of the marine fossil record.

RATIONALE: The impact of climate change on marine biodiversity depends on both its magnitude and on species' diverse biological sensi-

ties. Tolerances of marine animals to warming and O₂ loss are physiologically related and can be represented in a single metric: the ratio of temperature-dependent O₂ supply and demand rates. This ratio, termed the Metabolic Index (Φ), measures the environmental scope for aerobic activity and is governed by ocean conditions as well as thermal and hypoxia sensitivity traits that vary across species. If climate warming and O₂ loss reduce Φ below the species-specific minimum requirement for sustained ecological activity (Φ^{crit}), the ocean would no longer support active aerobic metabolism and, by extension, long-term population persistence.

RESULTS: We simulated the greenhouse gas-driven global warming at the end of the Permian using a model of Earth's climate and coupled biogeochemical cycles that matches geochemical proxy data. The imposed increase in atmospheric greenhouse gas levels raises near-

surface ocean temperatures by more than ~10°C and depletes global marine O₂ levels by almost 80%.

To predict the impact of these changes on animal habitat and survival, we measured the frequencies of Metabolic Index traits in diverse living species and used them to define a set of model ecophysiotypes. We populated the model Permian ocean with each ecophysiotype wherever conditions provide viable habitat ($\Phi \geq \Phi^{\text{crit}}$), yielding an ocean with diverse, locally adapted ecophysiotypes throughout all regions. Across the climate transition, however, ocean warming increases the metabolic O₂ demand amid declining supply; this removes large fractions of global aerobic habitat for the vast majority of ecophysiotypes and implies a high likelihood of extinction. We simulated the re-

ON OUR WEBSITE

Read the full article at <http://dx.doi.org/10.1126/science.aat1327>

sulting mass extinction of ecophysiotypes and found a robust geographic pattern: Extinction intensity should have been lower in the tropics than at high latitudes. The cause of lower tropical extinction is that organisms initially inhabiting these warm, low-O₂ environments can better exploit those conditions when they arise globally, whereas the habitats of more polar species disappear completely.

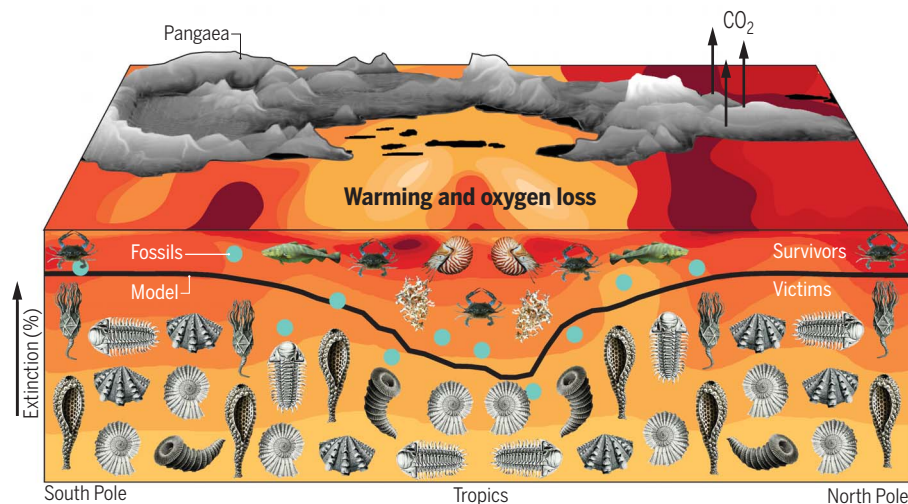
To test the geographic selectivity of the model extinction, we compared model predictions to spatially explicit reconstructions of genus extinction from the marine fossil record. We found that across diverse taxonomic groups, the observed extinction intensity indeed increases with latitude, consistent with the predicted signature of aerobic habitat loss. Comparison of the model to the fossil record implies that temperature-dependent hypoxia can account for more than half of the observed magnitude of regional extinction (i.e., extirpation).

CONCLUSION: Ocean warming and O₂ loss simulated in an Earth System Model of end-Permian climate change imply widespread loss of aerobic habitat among animal types with diverse thermal and hypoxia tolerances. The resulting extinctions are predicted to select most strongly against higher-latitude species, whose biogeographic niche disappears globally. The combined physiological stresses of ocean warming and O₂ loss largely account for the spatial pattern and magnitude of extinction observed in the fossil record of the "Great Dying." These results highlight the future extinction risk arising from a depletion of the ocean's aerobic capacity that is already under way. ■

The list of author affiliations is available in the full article online.

*Corresponding author. Email: jpenn@uw.edu (J.L.P.); cdeutsch@uw.edu (C.D.)

Cite this article as J. L. Penn et al., *Science* 362, eaat1327 (2018). DOI: 10.1126/science.aat1327



Schematic illustration of temperature-dependent hypoxia as a driver of the end-Permian marine mass extinction. Greenhouse gas forcing in a model of Earth's climate at the end of the Permian drives ocean warming (contours) and oxygen loss that match geochemical proxy data. Ocean warming raises the organismal O₂ demand amid declining supply. The resulting loss of aerobic habitat for diverse physiologies induces a mass extinction in model animal types (line) whose geographic signature—increased severity outside of the tropics—is consistent with reconstructions from the marine fossil record (circles).

RESEARCH ARTICLE

CLIMATE IMPACTS

Temperature-dependent hypoxia explains biogeography and severity of end-Permian marine mass extinction

Justin L. Penn^{1*}, Curtis Deutsch^{1,2*}, Jonathan L. Payne³, Erik A. Sperling³

Rapid climate change at the end of the Permian Period (~252 million years ago) is the hypothesized trigger for the largest mass extinction in Earth's history. We present model simulations of the Permian/Triassic climate transition that reproduce the ocean warming and oxygen (O₂) loss indicated by the geologic record. The effect of these changes on animal survival is evaluated using the Metabolic Index (Φ), a measure of scope for aerobic activity governed by organismal traits sampled in diverse modern species. Modeled loss of aerobic habitat predicts lower extinction intensity in the tropics, a pattern confirmed with a spatially explicit analysis of the marine fossil record. The combined physiological stresses of ocean warming and O₂ loss can account for more than half the magnitude of the "Great Dying."

Volcanic greenhouse gas release is widely hypothesized to have been the geological trigger for the largest mass extinction event in Earth's history at the end of the Permian Period [~252 million years (Ma) ago] (1, 2).

At least two-thirds of marine animal genera and a comparable proportion of their terrestrial counterparts were eliminated, but the mechanisms connecting environmental change to biodiversity collapse remain strongly debated. Geological and geochemical evidence points to high temperatures in the shallow tropical ocean (3, 4), an expansion of anoxic waters (5–8), ocean acidification (9–12), changes in primary productivity (13, 14), and metal (15) or sulfide (16, 17) poisoning as potential culprits. However, a quantitative, mechanistic framework connecting climate stressors to biological tolerance is needed to assess and differentiate among proposed proximal causes.

In this study, we tested whether rapid greenhouse warming and the accompanying loss of ocean O₂—the two best-supported aspects of end-Permian environmental change—can together account for the magnitude and biogeographic selectivity of end-Permian mass extinction in the oceans. Specifically, we simulated global warming across the Permian/Triassic (P/Tr) transition using a model of Earth's climate and coupled biogeochemical cycles, validated with geochemical data. We then used key physiological and ecological traits measured in a diverse group of extant species to predict the magnitude and distribution of habitat loss due to the temperature-

driven increase of metabolic O₂ demand amid declining supply (18). To assess the explanatory power of this model, we compared the predicted patterns of extinction to the global marine fossil record.

Climate warming and ocean O₂ loss

We simulated the P/Tr climate transition using the Community Earth System Model, which computes the exchanges of mass, energy, and momentum among interacting atmosphere, ocean, land surface, and sea ice components (19). Embedded in the ocean circulation are biogeochemical cycles of O₂, carbon, and nutrients driven by multiple plankton types. An initial climate state was equilibrated under low greenhouse gas concentrations and reconstructed paleogeography (19, 20). The model was then subjected to an instantaneous increase in greenhouse gas concentration that was sustained for 3000 years in order to reach a warm, near-equilibrium climate (fig. S1). The initial climate and subsequent radiative forcing were achieved by manipulating atmospheric pCO₂ (partial pressure of CO₂) across levels chosen to reproduce tropical ocean temperatures implied by isotopic proxy records (3, 4, 19, 21). Because the rate and timing of climate change, as well as the resulting biotic disturbance, are not precisely known, the analysis of model output was based on pre-disturbance and post-disturbance equilibrium states, which we refer to simply as Permian and Triassic, respectively.

The modeled Permian and Triassic climates are consistent with geological proxy data for ocean temperature. The imposed increase in atmospheric pCO₂ raises model near-surface temperatures by ~11°C in the Paleo-Tethys sea (Fig. 1A), consistent with reconstructions from the $\delta^{18}\text{O}$ of biogenic (conodont microfossil) apatite ($\delta^{18}\text{O}_{\text{apatite}}$; Fig. 1B). Modeled warming is

amplified in the near-surface ocean outside of the tropics (Fig. 1A) and throughout the upper ocean relative to the deep (Fig. 1C). Warming and fresh water input to the high-latitude surface ocean (fig. S2) together strengthen density stratification and weaken deep-water formation. From its near-modern state in the Permian, the meridional overturning circulation slows in the Triassic by more than 80% in both hemispheres (fig. S3). Deep ocean stagnation reaches its full extent after just ~300 years and persists unabated for the duration of the simulation (~3000 years).

The modeled Permian and Triassic climates are also consistent with geological proxies for marine anoxia. Abrupt warming and its attendant effects deplete the global marine O₂ inventory by ~76% (~140 mmol/m³), leading to extensive Triassic seafloor anoxia (Fig. 1D) that spans the entire northern portion of the Panthalassa Ocean and the eastern tropics, similar to the observed distribution of deeper-ocean sediments deposited under anoxic conditions [e.g., (6, 22)]. The global fraction of anoxic bottom water (f_{anox}) in the Permian (~0.1%) is close to modern values (~0.2%) but rises to ~40% in the Triassic (Fig. 1E), consistent with the expansion inferred from uranium isotopes in marine carbonates (7, 8).

O₂ loss is nearly complete in the abyss, but varies strongly with latitude throughout the upper ocean (Fig. 1F). At high latitudes, anoxia develops in waters as shallow as 150 m. In contrast, O₂ declines weakly or increases in portions of the tropical thermocline. This pattern of O₂ change cannot be explained by decreases in gas saturation alone. It requires additional changes in the cumulative loss of O₂ from microbial respiration below the surface ocean. Warming increases the rate of phytoplankton growth, whereas stratification increases their exposure to adequate sunlight, especially in high latitudes where deep convection and sea ice cover decline markedly. As a result, surface nutrients are drawn down in mid- and high latitudes and are exported in sinking particles to the deep sea (14), thereby reducing the nutrient supply to the tropical surface ocean (23) (fig. S4). This shift in nutrient distribution in turn lessens the microbial O₂ demand in the tropical thermocline, partially counteracting the lowered gas saturation and limiting O₂ loss, even while anoxia develops elsewhere.

Aerobic habitat loss

The effect of warming and O₂ loss on biodiversity in the end-Permian ocean depends not only on the magnitude and pattern of environmental change, but also on the sensitivities of marine animals. Tolerances to hypoxia and warming are physiologically related (24) and can be represented in a single metric, the Metabolic Index (Φ), derived from the ratio of temperature-dependent rates of O₂ supply and demand (18, 19):

$$\Phi = A_0 \frac{p\text{O}_2}{\exp\left[\frac{-E_a}{R_b} \left(\frac{1}{T} - \frac{1}{T_{\text{ref}}}\right)\right]} \quad (1)$$

¹School of Oceanography, University of Washington, Seattle, WA 98195, USA. ²Department of Biology, University of Washington, Seattle, WA 98195, USA. ³Department of Geological Sciences, Stanford University, Stanford, CA 94305, USA.

*Corresponding author. Email: jpenn@uw.edu (J.L.P.); cdeutsch@uw.edu (C.D.)

where pO_2 and T are the O_2 partial pressure and temperature of ambient water, respectively; k_B is Boltzmann's constant; and the parameters A_o (kPa^{-1}) and E_o (eV) represent fundamental physiological traits of a species. The inverse of A_o (i.e., $1/A_o$, in kPa) is the minimum pO_2 that can sustain the resting metabolic rate (i.e., the "hypoxic threshold") at a reference temperature (T_{ref}), and E_o is the temperature sensitivity of that threshold (Fig. 2A). The Metabolic Index measures the capacity of an environment to support aerobic activity by a factor of Φ above an organism's minimum requirement in a complete resting state ($\Phi = 1$). For both marine and terrestrial animals, the energy required for sustained activity (e.g., feeding, reproduction, defense) is elevated by a factor of ~ 1.5 to 7 above resting metabolic demand (18, 25) and represents an ecological trait, termed Φ^{crit} . If climate warming and O_2 loss reduce the Metabolic Index for an organism below its species-specific Φ^{crit} , the environment would no longer have the capacity to support active aerobic metabolism and, by extension, long-term population persistence.

We evaluated the range and frequency of traits governing the Metabolic Index across diverse modern species (19). Physiological traits ($1/A_o$ and E_o)

were estimated in 61 species that span benthic and pelagic habitats in all ocean basins across four phyla (Arthropoda, Chordata, Mollusca, and Cnidaria). The species include 28 malacostracans, 21 fishes, three bivalves and cephalopods, two copepods, and one each for gastropods, ascidians, scleractinian corals, and sharks (table S1); their range of body mass spans eight orders of magnitude. The ecological trait (Φ^{crit}) was estimated for 26 species with adequate biogeographical data. All parameters exhibited well-defined distributions reflecting the diversity and frequency of key metabolic traits among modern taxa at multiple levels of taxonomic hierarchy (fig. S5) (19).

We used the observed trait distributions to define a set of model ecophysiotypes and populate the model Permian ocean with each ecophysiotype wherever its traits and ocean conditions provide viable habitat ($\Phi \geq \Phi^{crit}$). Although modern species and the environments they encounter differ from those present during the Permian, the use of modern hypoxia traits to define Permian ecophysiotypes is grounded in two considerations. First, among well-sampled modern taxonomic groups, including arthropods, chordates, and mollusks, the distributions of hypoxia traits are not significantly different (fig. S5, B to D) (19).

This overlap of distributions implies a strong selective pressure for diverse physiological strategies for hypoxia tolerance and would apply to any cosmopolitan taxonomic group, including Permian phyla not well represented in our database. Second, the broad similarity in the temperature and O_2 conditions encountered today and in the simulated Permian climate (fig. S6) suggests that, whatever their other anatomical and physiological differences, the Permian aerobic environment should have selected for a range and frequency of hypoxia traits comparable to those of modern species. To test the adaptive suitability of modern trait diversity to the Permian ocean, we examined whether all ecophysiotypes find suitable habitat, and whether every region of the Permian ocean would be habitable by some subset of modern ecophysiotypes.

Variations in Permian environmental conditions and the three Metabolic Index traits give rise to a diverse set of biogeographic ranges (Fig. 2, B to D). For average physiological traits of the studied species ($1/A_o \sim 4.5$ kPa and $E_o \sim 0.4$ eV), Φ decreases with depth in the upper 1000 m but increases with latitude, restricting ecophysiotypes with higher ratios of active to resting metabolic rates to the extratropics (Fig. 2B). Because

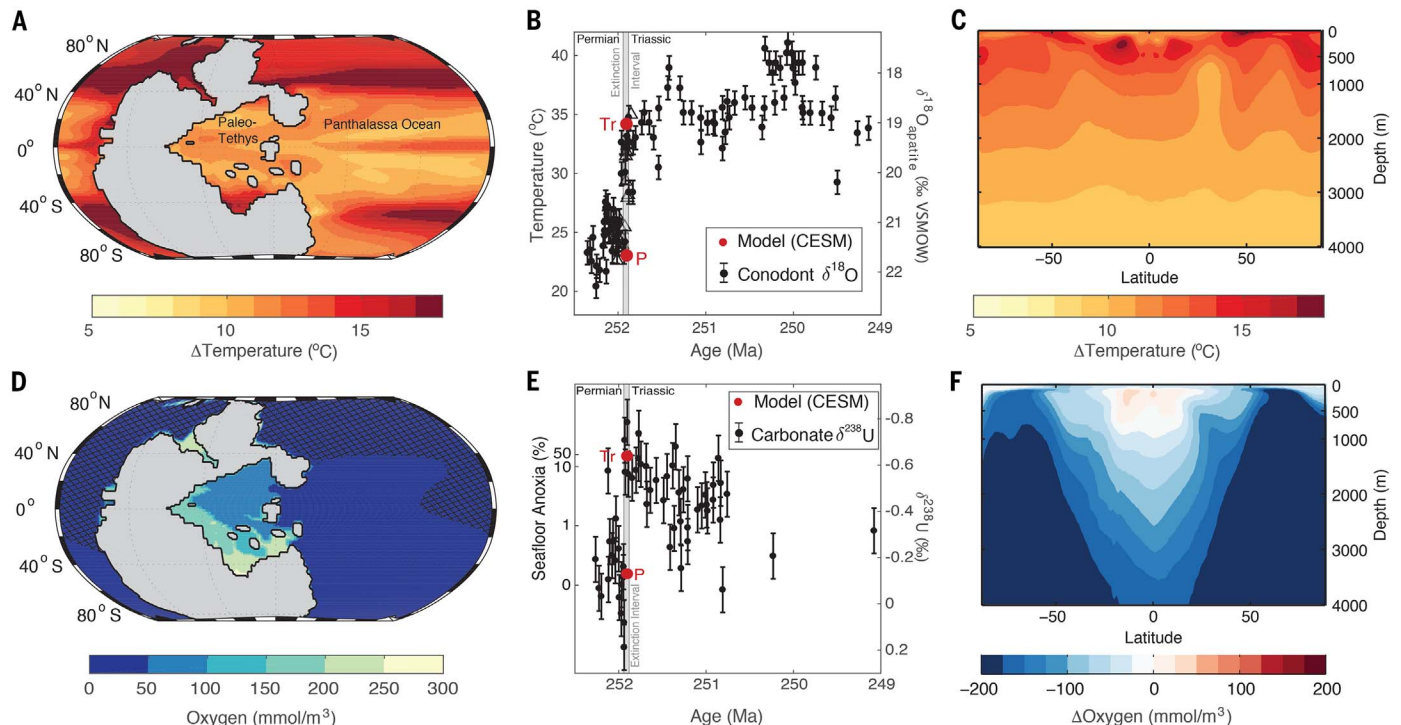


Fig. 1. Permian/Triassic ocean temperature and O_2 . (A) Map of near-surface (0 to 70 m) ocean warming across the Permian/Triassic (P/Tr) transition simulated in the Community Earth System Model. The region in gray represents the supercontinent Pangaea. (B) Simulated near-surface ocean temperatures (red circles) in the eastern Paleo-Tethys (5°S to 20°N) and reconstructed from conodont $\delta^{18}O_{apatite}$ measurements (black circles) (4). The time scale of the $\delta^{18}O_{apatite}$ data (circles) has been shifted by 700,000 years to align it with $\delta^{18}O_{apatite}$ calibrated by U-Pb zircon dates (open triangles) (1), which also define the extinction interval

(gray band). Error bars are $1^\circ C$. (C) Simulated zonal mean ocean warming ($^\circ C$) across the P/Tr transition. (D) Map of seafloor oxygen levels in the Triassic simulation. Hatching indicates anoxic regions ($O_2 < 5$ $mmol/m^3$). (E) Simulated seafloor anoxic fraction f_{anox} (red circles). Simulated values are used to drive a published one-box ocean model of the ocean's uranium cycle (8) and are compared to $\delta^{238}U$ isotope measurements of marine carbonates formed in the Paleo-Tethys (black circles). Error bars are 0.1‰ . (F) Same as in (C) but for simulated changes in O_2 concentrations ($mmol/m^3$).

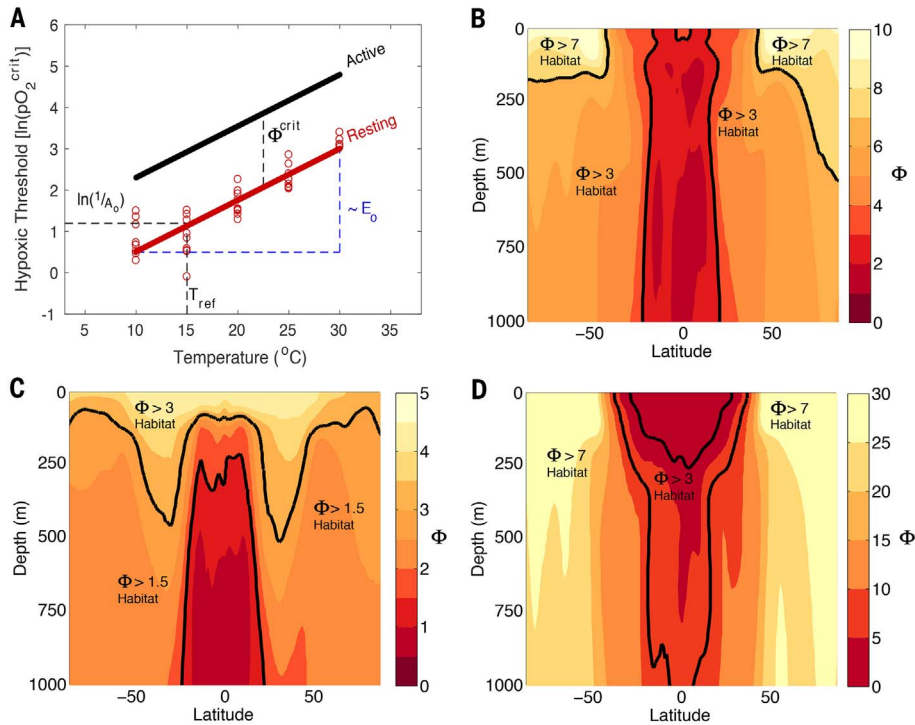


Fig. 2. Physiological and ecological traits of the Metabolic Index (Φ) and its end-Permian distribution. (A) The critical O_2 pressure (pO_2^{crit}) needed to sustain resting metabolic rates in laboratory experiments (red circles, *Cancer irroratus*) vary with temperature with a slope proportional to E_0 from a value of $1/A_0$ at a reference temperature (T_{ref}), as estimated by linear regression when $\Phi = 1$ (19). Energetic demands for ecological activity increase hypoxic thresholds by a factor Φ^{crit} above the resting state, a value estimated from the Metabolic Index at a species' observed habitat range limit. (B) Zonal mean distribution of Φ in the Permian simulation for ecophysiotypes with average $1/A_0$ and E_0 (~ 4.5 kPa and 0.4 eV, respectively). (C and D) Variations in Φ for an ecophysiotype with weak (C) and strong (D) temperature sensitivities ($E_0 = 0$ eV and 1.0 eV, respectively), both with $1/A_0 \sim 4.5$ kPa. Example values of Φ^{crit} (black lines) outline different distributions of available aerobic habitat for a given combination of $1/A_0$ and E_0 .

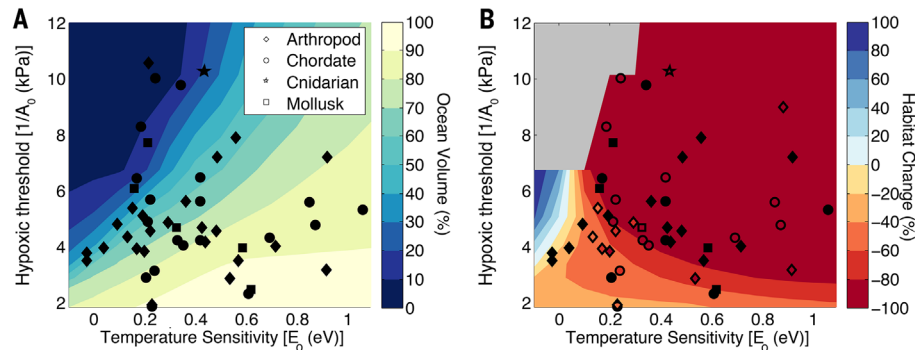


Fig. 3. Aerobic habitat during the end-Permian and its change under warming and O_2 loss. (A) Percentage of ocean volume in the upper 1000 m that is viable aerobic habitat ($\Phi \geq \Phi^{crit}$) in the Permian for ecophysiotypes with different hypoxic threshold parameters $1/A_0$ and temperature sensitivities E_0 . (B) Relative (percent) change in Permian aerobic habitat volume (ΔV_i , where i is an index of ecophysiotype) under Triassic warming and O_2 loss. Colored contours are for ecophysiotypes with $\Phi^{crit} = 3$. Measured values of $1/A_0$ and E_0 in modern species are shown as black symbols, but in (B) these are colored according to habitat changes at a species' specific Φ^{crit} where an estimate of this parameter is available. The gray region at upper left indicates trait combinations for which no habitat is available in the Permian simulation.

the hypoxic threshold scales the magnitude of Φ linearly (Eq. 1), variations in this parameter have an effect on the distribution of habitat similar to that of Φ^{crit} . In contrast, the temperature sensitivity parameter determines where Φ reaches its extreme values for a given distribution of temperature and O_2 (Fig. 2, C and D). For ecophysiotypes whose hypoxic thresholds are only weakly temperature-dependent ($E_0 < 0.1$ eV), Φ is maximized in the shallow low-latitude ocean (Fig. 2C). For the most temperature-sensitive ecophysiotypes ($E_0 \sim 1.0$ eV), Φ is greatest in the relatively cold waters of the high-latitude upper ocean and aerobic habitat expands with depth (Fig. 2D). The predicted niche partitioning leaves virtually no part of the Permian ocean uninhabited, partially confirming the relevance of modern trait diversity for the Permian.

Metabolic Index traits also have a strong impact on the predicted volume of available aerobic habitat (Fig. 3A). Ecophysiotypes with higher temperature sensitivities are able to inhabit the largest ocean volumes because most deep waters in the simulated Permian ocean are cold. In turn, ecophysiotypes with low hypoxic thresholds and/or low values of Φ^{crit} can occupy the largest ocean regions for a given temperature sensitivity. Simulated Permian habitat is available for $\sim 95\%$ of modern Metabolic Index trait combinations, both as global ocean volume (points in Fig. 3A) and as area on the seafloor (fig. S7A), further confirming that extant trait diversity is well adapted to the end-Permian ocean and is thus a sensible baseline for examining habitat loss and extinction.

Across the simulated climate transition, warming and O_2 loss remove a major fraction of aerobic habitat in the upper 1000 m for most ecophysiotypes (Fig. 3B) by lowering their metabolic indices below Φ^{crit} . The loss of habitat exceeds 90% for an ecophysiotype with the average traits; the vast majority ($\sim 95\%$) of ecophysiotypes experience declines, with magnitudes ranging from $\sim 20\%$ to 100% (fig. S8). Habitat loss preferentially selects against organisms with high hypoxic thresholds, high ratios of active to resting metabolic rates, and/or high temperature sensitivities. The former two traits impart low initial habitat volumes (Fig. 3A), whereas high temperature sensitivities amplify the decline in Φ per degree of warming. These patterns of differential habitat loss across ecophysiotypes are also found for coastal seafloor habitats (fig. S7B) and are qualitatively similar across ocean depth, but the average magnitude of habitat loss increases in the abyss because of the more complete O_2 loss (fig. S9).

Geography of global extinction

The severity of aerobic habitat loss predicted across the warming interval implies a high likelihood of extinction for many ecophysiotypes. We simulated the extinction of ecophysiotypes, defined by a fractional loss of global aerobic habitat volume (ΔV_i , where i indexes ecophysiotype) exceeding a specified critical threshold (V^{crit} ; Fig. 4A) (19), in waters above a maximum depth. Because maximum habitat depth and V^{crit} are poorly known ecological traits that are likely

Downloaded from <http://science.sciencemag.org/> on December 6, 2018

to vary across species, we computed the extinction across a wide range of values for these parameters. However, the geographical signature of the predicted mass extinction remains essentially the same irrespective of habitat depth and V^{crit} ; extinction intensity should have been lower for tropical communities than for those at higher latitudes.

The latitudinal gradient of extinction predicted from the Metabolic Index arises from the fundamental niche partitioning of Permian ecophysiotypes across latitude prior to the warming (Fig. 4B and fig. S10A). Ecophysiotypes with higher hypoxic thresholds and/or ratios of active to resting metabolisms are preferentially exterminated when the high latitudes warm and lose O_2 because they have no escape from inhospitable conditions. In contrast, ecophysiotypes whose Permian habitat includes the tropics must have traits pre-adapted to warm, low- O_2 environments and can better exploit these conditions when they arise globally. The extinction gradient is thus predicted to occur as long as the temperature-dependent hypoxia tolerance varies among ecophysiotypes, and as long as those with lower tolerance are confined to higher-latitude waters with a greater capacity to support aerobic activity. Under these conditions, the extinction pattern is only weakly dependent on the spatial gradients of climate warming and O_2 loss (fig. S10B), and holds regardless of the precise frequency distribution of Permian traits (figs. S10B, S11, and S12); the pattern also holds if habitat is defined by area on the seafloor or volume in the water column (fig. S13).

To test the predicted geographic selectivity of aerobic habitat loss, we compared the model extinction patterns to the reconstructed distribution of genus extinction across latitude (Fig. 4A and table S2) derived from fossil occurrences in the Paleobiology Database (19). The global mean magnitude of extinction estimated from the fossil compilation (~65% of genera) agrees with globally aggregated estimates (26) but displays a previously undescribed gradient across latitude, consistent with the model predictions. The observed extinction intensity increases by ~20% from the tropics to high latitudes, reaching at least 75% of genera outside of the tropics in both hemispheres. This trend is found in multiple taxonomic groupings, including those phyla with traits multiply sampled among modern taxa (arthropods, chordates, and mollusks) and in those that are not (fig. S14A). It is also robust to latitudinal differences in sampling intensity (fig. S14, B to D) and changes in the preservation of major depositional environments (fig. S15) (19). The correspondence between the simulated and observed geographic patterns of selectivity strongly implicates aerobic habitat loss, driven by rapid warming, as a main proximate cause of the end-Permian extinction.

Magnitude of regional extinction

Unlike the global extinction of ecophysiotypes, regional extinction (i.e., extirpation) in the model does not depend on V^{crit} or habitat depth. The

simulated extirpation is defined at a given location by the percentage of ecophysiotypes whose Metabolic Index is pushed below Φ^{crit} by Triassic climate change (19). Similar to global extinction, the extirpation of ecophysiotypes is elevated at higher latitudes but increases less systematically from the tropics (Fig. 4C). This pattern of ecophysiotype loss arises from the counteracting influences of global warming and O_2 loss on local aerobic habitat. Declining seawater O_2 concentrations drive extirpation in up to ~70% of ecophysiotypes in the high latitudes, but its impact diminishes to less than

~20% of ecophysiotypes in the tropics, where O_2 loss is weak (Fig. 1F). The effect of warming predicts the opposite pattern, with peak extirpation of ~65% at the equator dropping to ~20% at the poles. Local aerobic habitat is more sensitive per degree of warming in the tropics than in the high latitudes because Φ is already close to Φ^{crit} for the majority of Permian ecophysiotypes (Fig. 2, B to D). The realized impact of temperature on local habitat is therefore largest in the tropics because the pattern of upper-ocean warming is relatively constant across latitude (Fig. 1C), in contrast to the pattern of O_2 loss (Fig. 1F).

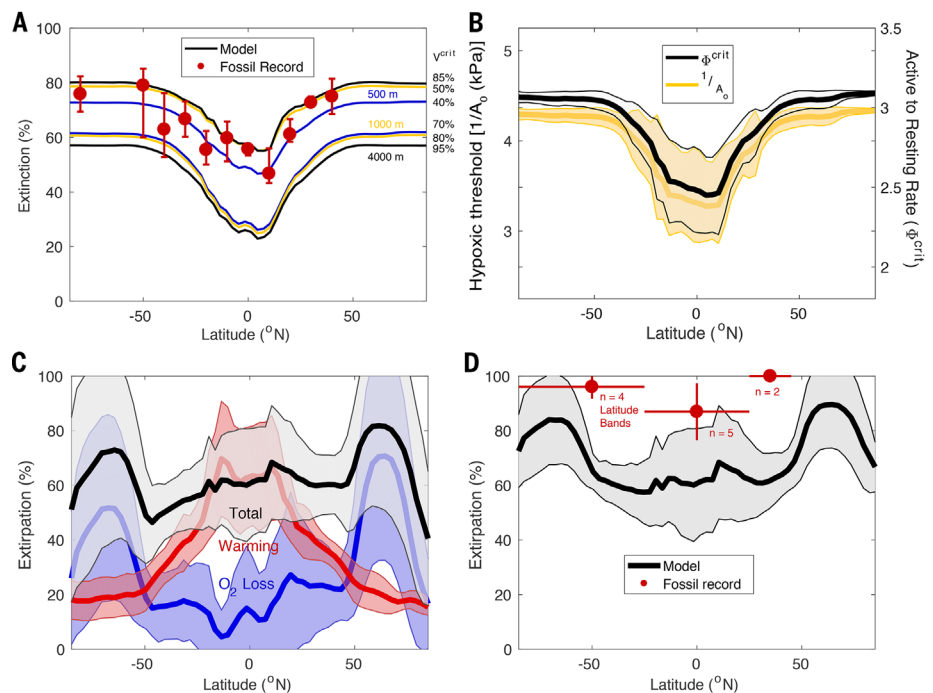


Fig. 4. Global and regional extinction at the end of the Permian. (A) Global extinction versus latitude, as predicted for model ecophysiotypes and observed in marine genera from end-Permian fossil occurrences in the Paleobiology Database (PBDB). Model extinction is calculated from the simulated changes in Permian global aerobic habitat volume (ΔV_i) under Triassic warming and O_2 loss (19). The maximum depth of initial habitat and fractional loss of habitat resulting in extinction (V^{crit}) are varied from 500 to 4000 m (colors) and from 40 to 95% (right-axis labels), respectively. The observed extinction of genera combines occurrences from all phyla in the PBDB (points). Error bars are the range of genera extinction across two taxonomic groupings: phyla multiply sampled in the modern physiology data (arthropods, chordates, and mollusks) and all other phyla. Latitude bands with fewer than five Permian fossil collections are excluded. The average range is used for latitude bands missing extinction estimates from both taxonomic groupings (i.e., 80°S, 30°S, and 40°N). The main latitudinal trend—increased extinction away from the tropics—is found when including all data together and when restricting to the best-sampled latitude bands (fig. S14). In all panels, model values are averaged across longitude and above 500 m. (B) Average hypoxic threshold and Φ^{crit} across ecophysiotypes versus latitude in the Permian. In (B) to (D), shading represents the 1σ standard deviation at each latitude. (C) Regional extinction (i.e., extirpation) versus latitude for model ecophysiotypes, with individual contributions from warming and the loss of seawater O_2 concentration. Extirpation occurs in locations where the Metabolic Index meets the active demand of an ecophysiotype in the Permian ($\Phi \geq \Phi^{\text{crit}}$) but falls below this threshold in the Triassic ($\Phi < \Phi^{\text{crit}}$). (D) Same as (C) but including globally extinct ecophysiotypes (using a maximum habitat depth of 1000 m and $V^{\text{crit}} = 80\%$), and as observed in marine genera from end-Permian and early Triassic fossil occurrences of all phyla in the PBDB. Observed extirpation magnitudes are averaged across tropical and extratropical latitude bands (red points and horizontal lines). Regional 1σ standard deviations are shown as vertical lines.

To test the predicted intensity of regional extinction, we used fossil occurrence data to estimate the extirpation of marine genera across the end-Permian extinction (19). The fossil extirpation intensities are more severe than fossil extinction intensities across all latitude bands (global mean $\sim 93\% \pm 8\%$ spatial SD) but show a similar gradient, increasing outside of the tropics (Fig. 4D). Extirpation exceeds extinction because not all locally lost genera disappeared globally, whereas all extinct genera were, by definition, extirpated everywhere. We can account for the effect of globally extinct ecophysiotypes in the model extirpation by using a combination of V^{crit} and habitat depth that predicts an equal contribution of aerobic habitat loss to both the observed regional and global extinction (19). Doing so increases the extirpation outside of the tropics, yielding a latitudinal gradient similar to the fossil data.

If we assume that the fossil occurrences primarily reflect habitat conditions above 500 m water depth (27), the global mean magnitude of ecophysiotype extirpation ($67\% \pm 18\%$ spatial SD) accounts for $\sim 72\%$ of the mean observed magnitude of genera extirpation (i.e., 93%; Fig. 4D). Including in this comparison the spatial variations in model extirpation yields a range explaining ~ 53 to 92% of the observed extirpation magnitude. Additional extinctions due to temperature-dependent hypoxia would have likely arisen from ecological interactions (28), including food web effects, because hypoxia-tolerant species could still be eliminated if they were dependent on hypoxia-vulnerable ones. Temperature-dependent hypoxia can thus account for the majority of biodiversity losses during the end-Permian mass extinction.

Discussion

Global warming and ocean O₂ loss were accompanied by other Earth system changes during the end-Permian crisis that likely added to the effects of temperature-dependent hypoxia. In our simulations, net primary productivity is reduced by $\sim 40\%$ globally, with strongest declines in the low latitudes, where essential nutrient supply to phytoplankton is most curtailed (fig. S4). Thus, acting alone, productivity losses would amplify extinction risk outside of the high latitudes, opposite to the pattern observed in the fossils.

Outgassing of CO₂ from the Siberian Traps would also have acidified the ocean (12), causing additional impacts via hypercapnia and/or reduced calcification (9, 29). These CO₂ effects are hypothesized to drive taxonomically selective extinctions, which may account for the $\sim 10\%$ lower mean genus extinction intensity for arthropods, chordates, and mollusks than for other less physiologically buffered phyla (fig. S14A). For the most heavily calcified animals in our modern trait dataset, the cold-water coral *Lophelia pertusa* and the scallop *Pecten maximus*, predicted losses of aerobic habitat are $\sim 94\%$ and $\sim 100\%$, respectively, suggesting a high extinction risk for calcifiers even without a direct CO₂ effect. Attributing taxonomically selective extinction (9, 29) to physiological mechanisms will require more metabolic trait

data, including from CO₂ effects on both calcification and aerobic habitat (hypercapnia), and from Permian phyla underrepresented in our database. However, the latitudinal gradient of extinction arising from the carbon cycle perturbation is unlikely to explain higher rates of tropical species persistence, for the same reason that hypoxia increases extinction at higher latitudes. Because the most corrosive waters are found poleward, species least tolerant of low pH or carbonate saturation would have been confined to the tropics and thus without refuge in an acidifying ocean.

The end-Permian mass extinction resulted in the largest loss of animal diversity in Earth's history, and its proposed geologic trigger—volcanic greenhouse gas release—is analogous to anthropogenic climate forcing. Predicted patterns of future ocean O₂ loss under climate change (30, 31) are broadly similar to those simulated here for the P/Tr boundary. Moreover, greenhouse gas emission scenarios projected for the coming centuries (32) predict a magnitude of upper ocean warming by 2300 CE that is ~ 35 to 50% of that required to account for most of the end-Permian extinction intensity. Given the fundamental nature of metabolic constraints from temperature-dependent hypoxia in marine biota, these projections highlight the potential for a future mass extinction arising from depletion of the ocean's aerobic capacity that is already under way.

REFERENCES AND NOTES

- S. D. Burgess, S. Bowring, S. Z. Shen, High-precision timeline for Earth's most severe extinction. *Proc. Natl. Acad. Sci. U.S.A.* **111**, 3316–3321 (2014). doi: [10.1073/pnas.1317692111](https://doi.org/10.1073/pnas.1317692111); pmid: [24516148](https://pubmed.ncbi.nlm.nih.gov/24516148/)
- J. L. Payne, M. E. Clapham, End-Permian mass extinction in the oceans: An ancient analog for the twenty-first century? *Annu. Rev. Earth Planet. Sci.* **40**, 89–111 (2012). doi: [10.1146/annurev-earth-042711-105329](https://doi.org/10.1146/annurev-earth-042711-105329)
- M. M. Joachimski et al., Climate warming in the latest Permian and the Permian-Triassic mass extinction. *Geology* **40**, 195–198 (2012). doi: [10.1130/G32707.1](https://doi.org/10.1130/G32707.1)
- Y. Sun et al., Lethally hot temperatures during the Early Triassic greenhouse. *Science* **338**, 366–370 (2012). doi: [10.1126/science.1224126](https://doi.org/10.1126/science.1224126); pmid: [23087244](https://pubmed.ncbi.nlm.nih.gov/23087244/)
- P. B. Wignall, R. J. Twitchett, Oceanic anoxia and the end Permian mass extinction. *Science* **272**, 1155–1158 (1996). doi: [10.1126/science.272.5265.1155](https://doi.org/10.1126/science.272.5265.1155); pmid: [8662450](https://pubmed.ncbi.nlm.nih.gov/8662450/)
- Y. Isozaki, Permo-Triassic boundary superanoxia and stratified superocean: Records from Lost Deep Sea. *Science* **276**, 235–238 (1997). doi: [10.1126/science.276.5310.235](https://doi.org/10.1126/science.276.5310.235); pmid: [9092467](https://pubmed.ncbi.nlm.nih.gov/9092467/)
- G. M. Brenneke, A. D. Herrmann, T. J. Algeo, A. D. Anbar, Rapid expansion of oceanic anoxia immediately before the end-Permian mass extinction. *Proc. Natl. Acad. Sci. U.S.A.* **108**, 17631–17634 (2011). doi: [10.1073/pnas.1106039108](https://doi.org/10.1073/pnas.1106039108); pmid: [21987794](https://pubmed.ncbi.nlm.nih.gov/21987794/)
- K. V. Lau et al., Marine anoxia and delayed Earth system recovery after the end-Permian extinction. *Proc. Natl. Acad. Sci. U.S.A.* **113**, 2360–2365 (2016). doi: [10.1073/pnas.1515080113](https://doi.org/10.1073/pnas.1515080113); pmid: [26884155](https://pubmed.ncbi.nlm.nih.gov/26884155/)
- A. H. Knoll, R. K. Bambach, J. L. Payne, S. Pruss, W. W. Fischer, Paleophysiology and end-Permian mass extinction. *Earth Planet. Sci. Lett.* **256**, 295–313 (2007). doi: [10.1016/j.epsl.2007.02.018](https://doi.org/10.1016/j.epsl.2007.02.018)
- J. L. Payne et al., Erosional truncation of uppermost Permian shallow-marine carbonates and implications for Permian-Triassic boundary events. *Bull. Geol. Soc. Am.* **119**, 771–784 (2007). doi: [10.1130/B26091.1](https://doi.org/10.1130/B26091.1)
- J. L. Payne et al., Calcium isotope constraints on the end-Permian mass extinction. *Proc. Natl. Acad. Sci. U.S.A.* **107**,

- 8543–8548 (2010). doi: [10.1073/pnas.0914065107](https://doi.org/10.1073/pnas.0914065107); pmid: [20421502](https://pubmed.ncbi.nlm.nih.gov/20421502/)
- M. O. Clarkson et al., Ocean acidification and the Permo-Triassic mass extinction. *Science* **348**, 229–232 (2015). doi: [10.1126/science.12589903](https://doi.org/10.1126/science.12589903); pmid: [25859043](https://pubmed.ncbi.nlm.nih.gov/25859043/)
- M. R. Rampino, K. Caldeira, Major perturbation of ocean chemistry and a "Strangelove Ocean" after the end-Permian mass extinction. *Terra Nova* **17**, 554–559 (2005). doi: [10.1111/j.1365-3121.2005.00648.x](https://doi.org/10.1111/j.1365-3121.2005.00648.x)
- S. E. Grasby, B. Beauchamp, J. Kries, Early Triassic productivity crises delayed recovery from world's worst mass extinction. *Geology* **44**, 779–782 (2016). doi: [10.1130/G38141.1](https://doi.org/10.1130/G38141.1)
- S. E. Grasby, H. Sanei, B. Beauchamp, Catastrophic dispersion of coal fly ash into oceans during the latest Permian extinction. *Nat. Geosci.* **4**, 104–107 (2011). doi: [10.1038/ngeo1069](https://doi.org/10.1038/ngeo1069)
- L. R. Kump, A. Pavlov, M. A. Arthur, Massive release of hydrogen sulfide to the surface ocean and atmosphere during intervals of oceanic anoxia. *Geology* **33**, 397–400 (2005). doi: [10.1130/G21295.1](https://doi.org/10.1130/G21295.1)
- K. Grice et al., Photic zone euxinia during the Permian-Triassic superanoxic event. *Science* **307**, 706–709 (2005). doi: [10.1126/science.1104323](https://doi.org/10.1126/science.1104323); pmid: [15661975](https://pubmed.ncbi.nlm.nih.gov/15661975/)
- C. Deutsch, A. Ferrel, B. Seibel, H. O. Pörtner, R. B. Huey, Climate change tightens a metabolic constraint on marine habitats. *Science* **348**, 1132–1135 (2015). doi: [10.1126/science.1256055](https://doi.org/10.1126/science.1256055); pmid: [26045435](https://pubmed.ncbi.nlm.nih.gov/26045435/)
- See supplementary materials.
- J. T. Kiehl, C. A. Shields, Climate simulation of the latest Permian: Implications for mass extinction. *Geology* **33**, 757–760 (2005). doi: [10.1130/G21654.1](https://doi.org/10.1130/G21654.1)
- C. Romano et al., Climatic and biotic upheavals following the end-Permian mass extinction. *Nat. Geosci.* **6**, 57–60 (2013). doi: [10.1038/ngeo1667](https://doi.org/10.1038/ngeo1667)
- E. A. Sperling, J. C. Ingle, A Permian-Triassic boundary section at Quinn River Crossing, northwestern Nevada, and implications for the cause of the Early Triassic chert gap on the western Pangean margin. *Bull. Geol. Soc. Am.* **118**, 733–746 (2006). doi: [10.1130/B25803.1](https://doi.org/10.1130/B25803.1)
- J. L. Sarmiento, N. Gruber, M. A. Brzezinski, J. P. Dunne, High-latitude controls of thermocline nutrients and low latitude biological productivity. *Nature* **427**, 56–60 (2004). doi: [10.1038/nature02127](https://doi.org/10.1038/nature02127); pmid: [14702082](https://pubmed.ncbi.nlm.nih.gov/14702082/)
- H. O. Pörtner, R. Knust, Climate change affects marine fishes through the oxygen limitation of thermal tolerance. *Science* **315**, 95–97 (2007). doi: [10.1126/science.1135471](https://doi.org/10.1126/science.1135471); pmid: [17204649](https://pubmed.ncbi.nlm.nih.gov/17204649/)
- C. C. Peterson, K. A. Nagy, J. Diamond, Sustained metabolic scope. *Proc. Natl. Acad. Sci. U.S.A.* **87**, 2324–2328 (1990). doi: [10.1073/pnas.87.6.2324](https://doi.org/10.1073/pnas.87.6.2324); pmid: [2315323](https://pubmed.ncbi.nlm.nih.gov/2315323/)
- S. M. Stanley, Estimates of the magnitudes of major marine mass extinctions in earth history. *Proc. Natl. Acad. Sci. U.S.A.* **113**, E6325–E6334 (2016). doi: [10.1073/pnas.1613094113](https://doi.org/10.1073/pnas.1613094113); pmid: [27698119](https://pubmed.ncbi.nlm.nih.gov/27698119/)
- H. Song et al., Anoxia/high temperature double whammy during the Permian-Triassic marine crisis and its aftermath. *Sci. Rep.* **4**, 4132 (2014). doi: [10.1038/srep04132](https://doi.org/10.1038/srep04132); pmid: [24549265](https://pubmed.ncbi.nlm.nih.gov/24549265/)
- P. D. Roopnarine, K. D. Angielczyk, S. C. Wang, R. Hertog, Trophic network models explain instability of Early Triassic terrestrial communities. *Proc. Biol. Sci.* **274**, 2077–2086 (2007). doi: [10.1098/rspb.2007.0515](https://doi.org/10.1098/rspb.2007.0515); pmid: [17609191](https://pubmed.ncbi.nlm.nih.gov/17609191/)
- A. H. Knoll, R. K. Bambach, D. E. Canfield, J. P. Grotzinger, Comparative Earth history and Late Permian mass extinction. *Science* **273**, 452–457 (1996). doi: [10.1126/science.273.5274.452](https://doi.org/10.1126/science.273.5274.452)
- R. J. Matear, A. C. Hirst, Long-term changes in dissolved oxygen concentrations in the ocean caused by protracted global warming. *Global Biogeochem. Cycles* **17**, 1125 (2003). doi: [10.1029/2002GB001997](https://doi.org/10.1029/2002GB001997)
- L. Bopp et al., Multiple stressors of ocean ecosystems in the 21st century: Projections with CMIP5 models. *Biogeosciences* **10**, 6225–6245 (2013). doi: [10.5194/bg-10-6225-2013](https://doi.org/10.5194/bg-10-6225-2013)
- M. Collins et al., *Climate Change 2013: The Physical Science Basis. Contribution of Working Group I to the Fifth Assessment Report of the Intergovernmental Panel on Climate Change* (Cambridge Univ. Press, 2013).

ACKNOWLEDGMENTS

We gratefully acknowledge the technical support of H. Frenzel, C. Bitz, and A. Winguth, data contributions from B. Seibel, and all those who contributed to the PaleoBiology Database, inspiration from R. Huey, the suggestions of three anonymous reviewers, and high-performance computing support from Yellowstone (ark:/85065/d7wd3hc) provided by NCAR's Computational and Information Systems Laboratory. **Funding:** Supported by grants from the

Gordon and Betty Moore Foundation (GBMF#3775) and NSF (OCE-1419323 and OCE-1458967). E.A.S. was supported by a Sloan Research Fellowship. **Author contributions:** C.D. initiated the study; J.L.Pe. designed and conducted model simulations; J.L.Pe. and C.D. analyzed model output; J.L.Pa. and E.A.S. analyzed fossil data; and J.L.Pe. and C.D. wrote the paper with input from all authors. **Competing interests:** The authors declare no competing interests. **Data and materials availability:** The locations of all data

used in this study are provided in the supplementary materials. Climate model output is available at Figshare; doi: 10.6084/m9.figshare.7357193.

SUPPLEMENTARY MATERIALS

www.sciencemag.org/content/362/6419/eaat1327/suppl/DC1
Materials and Methods

Supplementary Text
Figs. S1 to S15
Tables S1 to S3
References (33–71)

30 January 2018; accepted 19 October 2018
10.1126/science.aat1327

Temperature-dependent hypoxia explains biogeography and severity of end-Permian marine mass extinction

Justin L. Penn, Curtis Deutsch, Jonathan L. Payne and Erik A. Sperling

Science **362** (6419), eaat1327.
DOI: 10.1126/science.aat1327

Drivers of the "Great Dying"

Though our current extinction crisis is substantial, it pales in comparison to the largest extinction in Earth's history, which occurred at the end of the Permian Period. Referred to as the "Great Dying," this event saw the loss of up to 96% of all marine species and 70% of terrestrial species. Penn *et al.* explored the extinction dynamics of the time using Earth system models in conjunction with physiological data across animal taxa (see the Perspective by Kump). They conclude that increased marine temperatures and reduced oxygen availability were responsible for a majority of the recorded extinctions. Because similar environmental alterations are predicted outcomes of current climate change, we would be wise to take note.

Science, this issue p. eaat1327; see also p. 1113

ARTICLE TOOLS

<http://science.sciencemag.org/content/362/6419/eaat1327>

SUPPLEMENTARY MATERIALS

<http://science.sciencemag.org/content/suppl/2018/12/05/362.6419.eaat1327.DC1>

RELATED CONTENT

<http://science.sciencemag.org/content/sci/362/6419/1113.full>

REFERENCES

This article cites 69 articles, 28 of which you can access for free
<http://science.sciencemag.org/content/362/6419/eaat1327#BIBL>

PERMISSIONS

<http://www.sciencemag.org/help/reprints-and-permissions>

Use of this article is subject to the [Terms of Service](#)